Solar Physics (2021) 296:96
https://doi.org/10.1007/s11207-021-01841-1

Mixed Properties of Slow Magnetoacoustic and Entropy Waves in a Plasma with Heating/Cooling Misbalance

D. Zavershinskii[1,2] · D. Kolotkov[3,4] · D. Riashchikov[1,2] · N. Molevich[2]

Received: 5 March 2021 / Accepted: 24 May 2021 / Published online: 16 June 2021
© The Author(s), under exclusive licence to Springer Nature B.V. 2021

Abstract
The processes of coronal plasma heating and cooling were previously shown to significantly affect the dynamics of slow magnetoacoustic (MA) waves, causing amplification or attenuation, and also dispersion. However, the entropy mode is also excited in such a thermodynamically active plasma and is affected by the heating/cooling misbalance too. This mode is usually associated with the phenomenon of coronal rain and formation of prominences. Unlike adiabatic plasmas, the properties and evolution of slow MA and entropy waves in continuously heated and cooling plasmas get mixed. Different regimes of the misbalance lead to a variety of scenarios for the initial perturbation to evolve. In order to describe properties and evolution of slow MA and entropy waves in various regimes of the misbalance, we obtained an exact analytical solution of the linear evolutionary equation. Using the characteristic timescales and the obtained exact solution, we identified regimes with qualitatively different behaviour of slow MA and entropy modes. For some of those regimes, the spatio-temporal evolution of the initial Gaussian pulse is shown. In particular, it is shown that slow MA modes may have a range of non-propagating harmonics. In this regime, perturbations caused by slow MA and entropy modes in a low-β plasma would look identical in observations, as non-propagating disturbances of the plasma density (and temperature) either growing or decaying with time. We also showed that the partition of the initial energy between slow MA and entropy modes depends on the properties of the heating and cooling processes involved. The exact analytical solution obtained could be further applied to the interpretation of observations and results of numerical modelling of slow MA waves in the corona and the formation and evolution of coronal rain.

Keywords Waves, modes · Coronal seismology · Oscillations, solar

1. Introduction

In a series of recent works (Prasad, Srivastava, and Wang, 2021; Kolotkov, Duckenfield, and Nakariakov, 2020; Duckenfield, Kolotkov, and Nakariakov, 2021; Kolotkov, Nakariakov,

This article belongs to the Topical Collection:
Magnetohydrodynamic (MHD) Waves and Oscillations in the Sun's Corona and MHD Coronal Seismology
Guest Editors: Dmitrii Kolotkov and Bo Li

Extended author information available on the last page of the article

and Zavershinskii, 2019; Claes and Keppens, 2019; Zavershinskii et al., 2019), the thermodynamic activity of the solar corona, i.e. a wave-induced interplay between plasma heating and cooling processes, was shown to be among the most important physical processes affecting the dynamics of magnetoacoustic waves and oscillations in the corona. More specifically, a compressive wave violating coronal thermal equilibrium via perturbations of the local plasma parameters can experience a feedback from these unbalanced coronal-heating and -cooling processes, which is known as the phenomenon of thermal misbalance (Field, 1965; Molevich and Oraevskii, 1988; Nakariakov et al., 2017). In a broad range of typical physical conditions in the Sun's corona, the characteristic timescales of this thermal misbalance were shown to be about several minutes, which coincide with the oscillation periods of magnetoacoustic waves ubiquitously present in the coronal-plasma structures (see, e.g., Nakariakov and Kolotkov, 2020, for the most recent comprehensive review). In particular, the essentially compressive, slow-mode magnetoacoustic waves are confidently observed as propagating or standing disturbances in various coronal plasma non-uniformities such as, for example, polar plumes, quiescent and active-region loops, and they have oscillation periods ranging from a few to a few tens of minutes and comparable damping times (De Moortel, 2009; Banerjee, Gupta, and Teriaca, 2011; Wang, 2011; Banerjee and Krishna Prasad, 2016; Wang, 2016; Nakariakov et al., 2019; Wang et al., 2021). As such, slow waves are considered to be strongly affected by the process of thermal misbalance.

The direct observations and theoretical modelling of coronal slow waves are extensively used for seismological probing the coronal plasma. In particular, the effects of parallel thermal conduction and compressive viscosity, leading to a frequency- and temperature-dependent damping of slow waves and phase shifts between density and temperature perturbations, were measured by, e.g., Krishna Prasad, Banerjee, and Van Doorsselaere (2014), Wang et al. (2015, 2018), Krishna Prasad, Jess, and Van Doorsselaere (2019) and modelled by, e.g., Ofman and Wang (2002), De Moortel and Hood (2003), Selwa, Murawski, and Solanki (2005), Owen, De Moortel, and Hood (2009), Reale (2016), Mandal et al. (2016). An effective coronal polytropic index and its dependence on temperature were inferred seismologically with slow waves by Van Doorsselaere et al. (2011) and Krishna Prasad et al. (2018), respectively. Robust and reliable methods for measuring the apparent propagation speed of slow waves in legs of long, fan-like loops in active regions, as an important seismological tool, were designed by Yuan and Nakariakov (2012). Using a combination of the theory of the perturbed thermal equilibrium and observations of slow waves in long-lived coronal plasma structures, Kolotkov, Duckenfield, and Nakariakov (2020) seismologically constrained the parameters of the unknown coronal-heating function. Likewise, Reale et al. (2019) used observations of large-amplitude quasi-periodic pulsations associated with slow waves and a comprehensive theoretical modelling to diagnose duration of the impulsive coronal-heating events.

The feedback from the wave-induced thermal misbalance on the slow-wave dynamics is manifested, in particular, in the wave damping or amplification. Thus, Kolotkov, Nakariakov, and Zavershinskii (2019) demonstrated three possible regimes of the standing slow-wave evolution with enhanced damping (with respect to that caused by other dissipative processes, e.g. parallel thermal conduction) or suppressed damping and even amplification (over-stability) of the wave through the effective gain of energy from the heating source. It was shown that the observed rapid damping of standing slow oscillations in hot and dense coronal loops could be readily reproduced with a reasonable choice of the heating function. This study was generalised and extended by Duckenfield, Kolotkov, and Nakariakov (2021) for the effects of non-zero plasma-β and a broader range of coronal conditions. In the

over-stable regime, the effects of finite amplitude become important, leading to the distortion of the wave front and/or formation of autowave (self-sustained) shock pulses (Nakariakov, Mendoza-Briceño, and Ibáñez S., 2000; Chin et al., 2010; Zavershinsky and Molevich, 2013; Molevich, Zavershinskiy, and Ryashchikov, 2016; Nakariakov et al., 2017; Zavershinskii et al., 2020). The nonlinear evolution of slow magnetoacoustic waves in the corona was also addressed by, e.g., Ofman and Wang (2002), Ruderman (2006), Verwichte et al. (2008), Afanasyev and Nakariakov (2015), and Wang and Ofman (2019).

Zavershinskii et al. (2019) demonstrated another effect of the heating/cooling misbalance that is effective dispersion of slow waves. This additional misbalance-caused dispersion is manifested through the dependence of the wave phase and group speeds and effective polytropic index on the wave frequency; is fully attributed to the existence of the characteristic timescales of the misbalance process; and is not connected with the geometrical dispersion of magnetoacoustic waves, traditionally considered in the corona. Moreover, the slow-mode wave increment/decrement (i.e. damping/growth time or length, respectively) caused by the misbalance acquires the frequency dependence too, which is functionally different from that caused by the parallel thermal conduction and viscosity. In particular, accounting for this frequency-dependent damping by the misbalance in the model allowed Prasad, Srivastava, and Wang (2021) to better match the observed relationship between the oscillation period and damping time of the fundamental standing slow waves. Combining wave dispersion and frequency-dependent damping/amplification both associated with the effect of thermal misbalance, Zavershinskii et al. (2019) demonstrated formation of a quasi-periodic propagating slow magnetoacoustic wave train from the initially broadband aperiodic perturbation.

A particular regime, in which the wave evolves much faster/slower than the misbalance process does, corresponds to the weak/strong limits of the latter, respectively. Thus, in the regime of weak misbalance and low-β plasma, the slow-wave speed reduces to the standard adiabatic sound speed determined by the standard adiabatic index and the plasma temperature. In the regime of dominating misbalance, the wave becomes strongly non-adiabatic with a modified propagation speed and a new value of the effective polytropic index determined by the properties of the heat-loss processes. In both these regimes, the wave speeds are frequency-independent. This is similar to the theory of the lower and higher limits of parallel thermal conduction (see, e.g., Section 4.1 in Krishna Prasad, Banerjee, and Van Doorsselaere, 2014), for which the slow-wave speed varies between the adiabatic and isothermal values of the sound speed, respectively. A more general model of slow waves, including the combined effects of the weak/strong misbalance and lower/higher limits of thermal conduction that for uniformity was referred to as regimes of weak/strong non-adiabaticity, was considered by Duckenfield, Kolotkov, and Nakariakov (2021).

Another natural magnetohydrodynamic (MHD) process efficiently perturbing the coronal thermal equilibrium and strongly affected by the back-reaction of this perturbation is the entropy wave. It is a non-propagating compressive mode (see, e.g., Somov, Dzhalilov, and Staude, 2007; Murawski, Zaqarashvili, and Nakariakov, 2011), either growing or decaying in response to the violation of the balance between plasma heating and cooling processes (Field, 1965). In particular, the radiative instability of the entropy mode could lead to rapid condensations of the coronal plasma and formation of coronal rain (see, e.g., Antolin, 2020, and the references therein, for the most recent review) or prominences (e.g. Kaneko and Yokoyama, 2017). Hence, in a continuously heated and cooling plasma of the solar corona, the properties and evolution of entropy waves and slow magnetoacoustic waves could get mixed through the mechanism of thermal misbalance, even in the linear regime. The question of mixed properties of MHD waves in the solar corona is usually considered in the context of radial fundamental kink modes and Alfvén waves in coronal loops (see, e.g.,

Goossens, Arregui, and Van Doorsselaere, 2019, for a recent work), while the mixed properties of slow magnetoacoustic and entropy waves in the coronal plasma with heating/cooling misbalance has not been addressed in the previous theoretical or observational work.

In this article, we perform a comprehensive, analytical treatment of slow magnetoacoustic and entropy waves, simultaneously excited and evolving in the linear regime in a thermodynamically active plasma of the solar corona, by obtaining an exact analytical solution of the evolutionary equation (see Section 2 – 4). This exact analytical solution for the linear wave dynamics in a plasma with thermal misbalance is derived for the first time in this work. Unlike the previous work (e.g. Kolotkov, Nakariakov, and Zavershinskii, 2019; Zavershinskii et al., 2019) that considered the characteristic timescales of the thermal misbalance to be strictly positive to avoid the instability of the entropy mode, the novel element of the present work is that we do not use this assumption. Indeed, the estimations of the characteristic misbalance time for typical coronal conditions (see, e.g., Table 2 and Figure 3 in Kolotkov, Duckenfield, and Nakariakov, 2020) have shown that it could be both positive and negative, depending on the properties of the heat-loss function. Taking these negative times into account in this work allows us, in particular, to reveal the range of non-propagating slow magnetoacoustic harmonics, which are thereby not obviously distinguishable from the harmonics of the entropy wave. Revealing a specific regime of thermal misbalance in which slow magnetoacoustic harmonics may become non-propagating and thus possess properties similar to those of the entropy waves is another new result of this work. Using the obtained analytical solution, we describe and demonstrate different scenarios of the slow and entropy wave spatio-temporal evolution (Section 5.1). We stress that the individual dynamics of those waves cannot be analysed by solving the original evolutionary equation numerically, which allows for obtaining the dynamics of their superposition only. In Section 5.2, we demonstrate partition of the energy of the initial perturbation between slow and entropy waves, as another manifestation of their mixed properties. For example, this issue cannot be resolved from the analysis of the dispersion relation and requires an exact solution of the evolutionary equation obtained in this work. The dependence of the partition of the initial perturbation energy between slow magnetoacoustic and entropy modes on the coronal-heating and -cooling processes is demonstrated for the first time in this work. The discussion of the results and conclusions is given in Section 6.

2. Governing Wave equation

The linear dynamics of slow magnetoacoustic (MA) and entropy waves in a uniform-along-the-field plasma with the heating/cooling misbalance is described by the following evolutionary equation, derived in the infinite-field approximation by Zavershinskii et al. (2019):

$$\frac{\partial^3\rho_1}{\partial t^3}-c_{\rm S}^2\frac{\partial^3\rho_1}{\partial t\partial z^2}=\frac{\kappa}{\rho_0 C_{\rm V}}\left(\frac{\partial^4\rho_1}{\partial z^2\partial t^2}-c_{\rm S0}^2\frac{\partial^4\rho_1}{\partial z^4}\right)-\frac{1}{\tau_2}\left(\frac{\partial^2\rho_1}{\partial t^2}-c_{\rm SQ}^2\frac{\partial^2\rho_1}{\partial z^2}\right). \tag{1}$$

The two terms on the RHS of Equation 1 describe the effects of the field-aligned thermal conduction with the coefficient κ and thermal misbalance on small-amplitude plasma density perturbations ρ_1. More specifically, $c_{\rm S}=\sqrt{\gamma {\rm k_B} T_0/m}$ and $c_{\rm S0}=\sqrt{{\rm k_B}T_0/m}$ are the standard adiabatic (with the adiabatic index γ) and isothermal sound speeds, respectively; $c_{\rm SQ}=\sqrt{\gamma_Q {\rm k_B}T_0/m}$ is the sound speed of wave propagation in the regime of strong misbalance (when the second term on the RHS of Equation 1 dominates), prescribed by the

effective polytropic index $\gamma_Q \equiv Q_{[P]T}/Q_{[\rho]T} = \gamma\tau_2/\tau_1$ (Heyvaerts, 1974; Molevich and Oraevskii, 1988) and the characteristic timescales of the misbalance,

$$\tau_1 = C_P/Q_{[P]T}, \tag{2}$$

$$\tau_2 = C_V/Q_{[\rho]T}. \tag{3}$$

Here, $Q_{[P]T}$ and $Q_{[\rho]T}$ are the derivatives of the combined heat $[H]$ and loss $[L]$ function

$$Q(\rho, T) = L(\rho, T) - H(\rho, T), \tag{4}$$

with respect to the plasma temperature $[T]$, taken at the constant gas pressure P and density ρ, i.e. $Q_{[\rho]T} = (\partial Q/\partial T)_\rho$, $Q_{[P]T} = (\partial Q/\partial T)_P = (\partial Q/\partial T)_\rho - (\rho_0/T_0)\,(\partial Q/\partial\rho)_T$. In this notation, k_B is the Boltzmann constant, m is the mean particle mass, and C_P and C_V are specific heat capacities at constant pressure and volume, respectively.

As an initial equilibrium, we consider a long-lived coronal plasma with density ρ_0 and temperature T_0, and with the radiative cooling and heating rates balancing each other, so that $Q_0(\rho_0, T_0) = 0$. As seen from Equation 1, the effects caused by the linear wave perturbation of such a thermal equilibrium (wave-induced thermal misbalance) are determined not by the sign and absolute value of Q, but by the sign and absolute values of its derivatives [$Q_{[P]T}$ and $Q_{[\rho]T}$] or, equivalently, by the characteristic times [$\tau_{1,2}$]. Previous estimations by Kolotkov, Duckenfield, and Nakariakov (2020) showed that for typical coronal conditions these timescales can be either positive or negative depending on a specific form of the heat-loss function [$Q(\rho, T)$.] From the physical standpoint, those thermal-misbalance timescales [τ_1 and τ_2] are the main parameters determining the effect of the perturbed thermal equilibrium on the wave dynamics described by Equation 1, which demonstrates how quickly the plasma restores its initial thermal equilibrium or becomes thermodynamically unstable.

The infinite magnetic-field approximation used for obtaining Equation 1 implies the magnetic-field strength is high enough to neglect its perturbations by the slow MA wave and hence to consider the wave dynamics as one-dimensional, strictly along the field. Its applicability to slow MA waves in the solar corona was recently justified by Duckenfield, Kolotkov, and Nakariakov (2021), for the magnetic-field strength greater than 10 G in the quiescent loops and polar plumes and greater than 100 G in hot and dense loops in active regions. In these cases, the potential dependence of the unknown coronal-heating function on the magnetic-field strength was shown to have no effect on the wave dynamics. Hence, without loss of generality in our work this dependence is omitted in Equation 1. Also, the effects of the gravitational stratification of the coronal plasma are missing in Equation 1, which is consistent with the physical conditions in, e.g., hot and dense loops for which the characteristic stratification scale height is known to be much greater than a typical loop height (see, e.g., Wang et al., 2018; Wang and Ofman, 2019). In this work, we use Equation 1 originally obtained by Zavershinskii et al. (2019) as a starting point, without re-deriving it. Being third-order with respect to time, Equation 1 describes three wave modes, which are two slow MA modes and one entropy mode.

In addition to the assumptions described above, the most recent seismological studies with slow waves revealed evidence of strong suppression of the parallel thermal conduction at least in some solar active regions (see a series of works by Wang et al., 2015, 2018; Wang and Ofman, 2019). Likewise, Nisticò et al. (2017) obtained seismologically the effective adiabatic index of about 5/3 in a hot loop hosting a slow-mode oscillation, which could also be considered as an indirect evidence of a diminished efficiency of the parallel thermal conduction. Moreover, observations by Krishna Prasad et al. (2018) showed the increase in

the effective coronal polytropic index with temperature, which is also inconsistent with the theoretical prediction arising from the effect of thermal conduction. Addressing these recent observational precedents of anomalously low thermal conduction, in this work we neglect the first term on the RHS of Equation 1.

Thus, the main equation governing the linear evolution of slow MA and entropy waves in a plasma with heating/cooling misbalance and under the assumptions described above is

$$\frac{\partial^3 \widetilde{\rho}}{\partial \tilde{t}^3} - \gamma \frac{\partial^3 \widetilde{\rho}}{\partial \tilde{t} \partial \tilde{z}^2} = -\widetilde{\nu}_2 \left(\frac{\partial^2 \widetilde{\rho}}{\partial \tilde{t}^2} - \gamma_Q \frac{\partial^2 \widetilde{\rho}}{\partial \tilde{z}^2} \right). \tag{5}$$

Here, we have introduced the dimensionless density perturbation [$\tilde{\rho} = \rho_1/\rho_0$], coordinate [$\tilde{z} = z/L$], and time [$\tilde{t} = t c_{S0}/L$], where L is the characteristic spatial scale of the medium (for example, the loop length). Also, hereafter we use dimensionless characteristic frequencies $\tilde{\nu}_1$, $\tilde{\nu}_2$, and $\tilde{\nu}_{12}$, defined through the characteristic thermal-misbalance timescales [τ_1 and τ_2] as

$$\widetilde{\nu}_{1,2} = \frac{1}{\widetilde{\tau}_{1,2}} = \frac{L}{\tau_{1,2} c_{S0}}, \quad \widetilde{\nu}_{12} = \frac{\widetilde{\tau}_1 - \widetilde{\tau}_2}{2\widetilde{\tau}_2 \widetilde{\tau}_1}. \tag{6}$$

In Section 3, we demonstrate that depending on the ratio, sign, and absolute values of the characteristic thermal-misbalance times [$\tau_{1,2}$] (or their dimensionless counterparts [$\widetilde{\nu}_{1,2}$ and $\widetilde{\nu}_{12}$]), the harmonics of slow MA and entropy waves may evolve differently. Further analysis is conducted for dimensionless quantities, hence the tilde sign is omitted.

3. Parametric Analysis

We obtain the solution for the evolutionary Equation 5 by the separation of variables that is also known as the Fourier method. A perturbation of the plasma equilibrium state can, in general, be represented as a sum of the wave modes constituting it (in our case a sum of the entropy and slow MA modes). The Fourier method allows us to distinguish between the impact of these different physical modes, determine partition of the energy of the initial perturbation between them, and analyse their evolution separately. Moreover, this method allows us to analyse the behaviour of the individual Fourier harmonics of those physical modes, which may grow or decay, and propagate or not propagate. The latter non-propagating behaviour is retained across the whole spectrum of the perturbation for entropy waves and may occur in a specific interval of harmonics for slow MA waves. For example, in the discussed coronal plasma with thermal misbalance, some harmonics of the slow MA mode may grow and propagate, while other harmonics of the same mode may also grow but not propagate, if certain physical conditions are fulfilled. In this section, we derive those conditions explicitly for both the slow MA and the entropy modes and link them with the characteristic timescales of the misbalance: $\tau_{1,2}$ (Equations 2 and 3).

3.1. Behaviour of the Individual Fourier Harmonics

Applying the Fourier method, we search for the solution for Equation 5 of the form $\rho(z,t) = \varphi(z)\,\psi(t)$. This substitution allows us to split Equation 5 into two equations describing dependence of the full solution on coordinate [$\varphi(z)$] and on time [$\psi(t)$], respectively.

The equation describing the dependence of the perturbation on coordinate $[\varphi(z)]$ has the form of a harmonic oscillator,

$$\frac{\mathrm{d}^2\varphi}{\mathrm{d}z^2} + k^2\varphi = 0, \tag{7}$$

where k^2 are the eigenvalues that appear after the separation of variables in Equation 5 as $F_1(\psi, \psi_t', \psi_{tt}'', \psi_{ttt}''') = F_2(\varphi, \varphi_{zz}'') = -k^2$. We assume that there are no mass flows at the boundaries, which implies that Neumann boundary conditions $\partial\rho(0,t)/\partial z = \partial\rho(l,t)/\partial z = 0$, or equivalently $\mathrm{d}\varphi(0)/\mathrm{d}z = \mathrm{d}\varphi(l)/\mathrm{d}z = 0$, are applied. Here, l is the length of the medium normalised to the characteristic length scale L.

The oscillatory solutions of Equation 7 exist only for eigenvalues $k^2 > 0$. In this case, the eigenvalues k can be defined by the harmonic number n as

$$k = \frac{\pi n}{l}, n = 1, 2, 3, ... \tag{8}$$

The eigenvalues (Equation 8) correspond to the set of possible wavenumbers of the entropy and slow MA modes, which in turn defines the set of possible wavelengths $\lambda = 2\pi/k$. The quantisation of the wavenumbers $[k]$ in terms of the characteristic length of the medium $[l]$ implies the existence of a closed resonator (for example, the coronal loop), which would eventually allow the initially localised MA perturbation to form standing waves if it does not dissipate or leak out before getting reflected from the resonator boundary. On the other hand, the developed theory can be readily applied for description of propagating waves in open plasma structures too, if the wave travel time to the resonator boundary is longer than its lifetime or by the use of open boundary conditions. In this case, the set of wavenumbers $[k]$ would be continuous and fully prescribed by the driver.

The solution of Equation 7 for $k^2 > 0$ and the chosen boundary conditions is well-known and gives us the spatial dependencies $[\varphi(z) = \varphi_n(z)]$ for $n > 0$ of the full solution $[\rho(z,t)]$. The particular case with $k^2 = 0$ $(n = 0)$ corresponds to a non-oscillatory background of the full solution $[\rho_0(z,t)]$ with spatial dependence $\varphi_0(z)$.

In order to describe temporal evolution of the entropy and slow MA harmonics with wavenumbers $k^2 > 0$, we consider the equation for $\psi(t)$, arising from the same separation of variables procedure. This equation is the third-order, linear, ordinary differential equation with constant coefficients written as

$$\frac{\mathrm{d}^3\psi}{\mathrm{d}t^3} + \nu_2\frac{\mathrm{d}^2\psi}{\mathrm{d}t^2} + k^2(n)\gamma\frac{\mathrm{d}\psi}{\mathrm{d}t} + k^2(n)\gamma_Q\nu_2\psi = 0. \tag{9}$$

The solution of Equation 9 may have different forms (see, e.g., Polyanin and Zaitsev, 2002), depending on the type of roots of the following cubic algebraic equation:

$$\omega^3 - \mathrm{i}\nu_2\omega^2 - k^2(n)\gamma\omega + \mathrm{i}k^2(n)\gamma_Q\nu_2 = 0, \tag{10}$$

obtained by writing $\mathrm{d}/\mathrm{d}t \to \mathrm{i}\omega$ in Equation 9. The cubic equation with complex coefficients (Equation 10) coincides with the general dispersion relation for slow and entropy modes in the plasma with thermal misbalance, derived by, e.g., Field (1965), Ryashchikov, Molevich, and Zavershinskii (2017), Zavershinskii et al. (2019), and Kolotkov, Nakariakov, and Zavershinskii (2019). Thus, roots of Equation 10 can be considered as complex frequencies $[\omega_{1,2,3}]$ of entropy and slow MA harmonics, corresponding to real wavenumber $[k]$. The asymmetry in the temporal and spatial dependencies (powers of ω and k) described by

Equation 10 can be explained by the fact that out of all three possible solutions only two slow MA modes can propagate. The phase speed of the entropy mode is always equal to zero.

The discriminant Δ of Equation 10 is

$$\Delta = -108(R^3 + U^2), \tag{11}$$

where R and U are real coefficients,

$$R = \frac{3k^2\gamma - \nu_2^2}{9}, \quad U = \frac{2\nu_2^3 - 9\nu_2 k^2\gamma + 27k^2\gamma_Q\nu_2}{54}.$$

Thus, as the discriminant Δ (Equation 11) is purely real-valued, frequencies $\omega_{1,2,3}$ may have the following types for given k:

i) *Case 1* with one purely imaginary root $[\omega_1]$ and two complex conjugate roots $[\omega_{2,3}]$. This case is physically equivalent to the existence of one non-propagating (entropy) harmonic and two propagating (slow MA) harmonics.
ii) *Case 2* with all three roots $[\omega_{1,2,3}]$ being purely imaginary. In this case, not only the entropy harmonic but also two slow MA harmonics become non-propagating.

Occurrence of *Cases 1,2* directly depends on the sign and absolute values of the constant coefficients in Equation 10. In our problem, they are defined not only by the harmonic number n, but, more importantly, by the properties of the heat-loss function $Q(\rho, T)$ through the quantities $\gamma_Q = \gamma\tau_2/\tau_1$ (Equations 2 and 3) and $\nu_2 = L/(\tau_2 c_{S0})$ (Equation 6). In other words, for some chosen heat-loss function $Q(\rho, T)$ providing fixed values of the timescales τ_1 and τ_2 (and their combinations γ_Q and ν_2), *Case 1* (with one non-propagating and two propagating harmonics) does not necessarily hold true for all harmonic numbers n in the perturbation spectrum. Thus, the possibility for certain MA harmonics excited in a thermodynamically active plasma of the solar corona to propagate or not propagate directly depends on the coronal heat-loss function $[Q(\rho, T)]$.

According to Cardano's formula, the roots of the dispersion relation (Equation 10) can be written as

$$\begin{aligned}
\omega_1 &= \mathrm{i}\left(-\frac{\nu_2}{3} + A + B\right), \\
\omega_2 &= \frac{A-B}{2}\sqrt{3} - \mathrm{i}\left(\frac{\nu_2}{3} + \frac{A+B}{2}\right), \\
\omega_3 &= -\frac{A-B}{2}\sqrt{3} - \mathrm{i}\left(\frac{\nu_2}{3} + \frac{A+B}{2}\right),
\end{aligned} \tag{12}$$

where

$$A = \sqrt[3]{-U + \sqrt{-\Delta/108}}, \quad B = -R/A.$$

We can discriminate between *Cases 1,2*, using discriminant Δ (Equation 11) and roots $\omega_{1,2,3}$ (Equation 12) for a given harmonic number n. Thus, *Case 1* occurs for $\Delta < 0$. Taking a real-valued cubic root in the expression for the coefficient A in Equation 12, we can determine the type of roots $[\omega_{1,2,3}]$ and uniquely associate them with the physical wave modes. In this case, the frequency ω_1 is purely imaginary and the conjugate frequencies $\omega_{2,3}$ are complex. This corresponds to a non-propagating entropy harmonic with the number n, which has

zero real part [$\omega_{\rm ER} = 0$] and non-zero imaginary part [$\omega_{\rm EI} \neq 0$] (i.e. increment/decrement) of the frequency ω_1,

$$\omega_{\rm EI} = -\frac{\nu_2}{3} + A + B. \tag{13}$$

In addition, there are two slow MA harmonics propagating in the opposite directions with the same number n. They have non-zero real part [$\omega_{\rm AR} \neq 0$] and non-zero imaginary part [$\omega_{\rm AI} \neq 0$] (i.e. increment/decrement) of the complex conjugate frequencies $\omega_{2,3} = \pm\omega_{\rm AR} - {\rm i}\omega_{\rm AI}$. From Equation 12, those MA real and imaginary parts are

$$\omega_{\rm AI} = \frac{\nu_2}{3} + \frac{A+B}{2}, \quad \omega_{\rm AR} = \frac{A-B}{2}\sqrt{3}. \tag{14}$$

Case 2 with three purely imaginary roots $\omega_{1,2,3}$ (Equation 12), corresponding to one non-propagating entropy harmonic and two non-propagating slow MA harmonics, occurs for $\Delta > 0$. In this case, all values of the cubic root in the expression for the coefficient A are complex. It can be shown that for this case both slow MA and entropy harmonics have zero real part of the frequency $\omega_{\rm AR} = \omega_{\rm ER} = 0$. However, all modes have non-zero imaginary parts $\omega_{\rm AI}$, $\omega_{\rm EI} \neq 0$ (i.e. increment/decrements), coinciding with the imaginary roots $\omega_{1,2,3}$ (Equation 12). In this regime, perturbations of the plasma density and/or temperature caused by slow MA and entropy harmonics with the same wavenumber [$k(n)$] would look identical, as a non-propagating disturbance either growing or decaying with time. In other words, it is not always obvious to distinguish between the physical modes of a slow MA or entropy nature in the set of roots $\omega_{1,2,3}$ (Equation 12) in *Case 2*. On the other hand, for varying properties of the heat-loss function [$Q(\rho, T)$], i.e. different values of the parameters τ_1 and τ_2, one of those imaginary roots can change sign (causing the corresponding physical mode to be stable or unstable) independently of the two other imaginary roots. In the following analysis, we use this property as a rule of thumb to differentiate between slow MA and entropy modes among the roots $\omega_{1,2,3}$ (Equation 12) in *Case 2*.

Thus, using Equations 12 – 14 we can write conditions for the plasma modes to amplify/attenuate (be unstable/stable), in terms of the characteristic misbalance times τ_1 and τ_2 (Equations 2 and 3). These conditions are visualised for the entropy and slow MA (both propagating and non-propagating) modes in the left-hand panel of Figure 1. In this work, we analyse the dependence of the roots $\omega_{1,2,3}$ (Equation 12) on the characteristic times numerically, i.e. we numerically search for the real and imaginary parts of $\omega_{1,2,3}$ for all possible values of $\tau_{1,2}$ (from $-\infty$ to $+\infty$).

The slow MA waves amplify (become unstable) if the imaginary part of two frequencies in the set of roots (Equation 12) is negative regardless of the sign of the increment/decrement of the other root, thus associated with the entropy wave, for all harmonic numbers n. As shown by Figure 1, this condition is satisfied in three distinct regions of positive and negative $\tau_{1,2}$. These regions coincide with the isentropic instability condition for slow MA modes introduced by Field (1965) and written in terms of the characteristic times $\tau_{1,2}$ by Zavershinskii et al. (2019) and Kolotkov, Nakariakov, and Zavershinskii (2019) as

$$\frac{\tau_1 - \tau_2}{\tau_1 \tau_2} < 0, \tag{15}$$

in the limit of weak dispersion.

Similarly, the entropy mode is considered to amplify (become unstable), if the imaginary part of one of three roots (Equation 12) is negative regardless of the sign of the other two

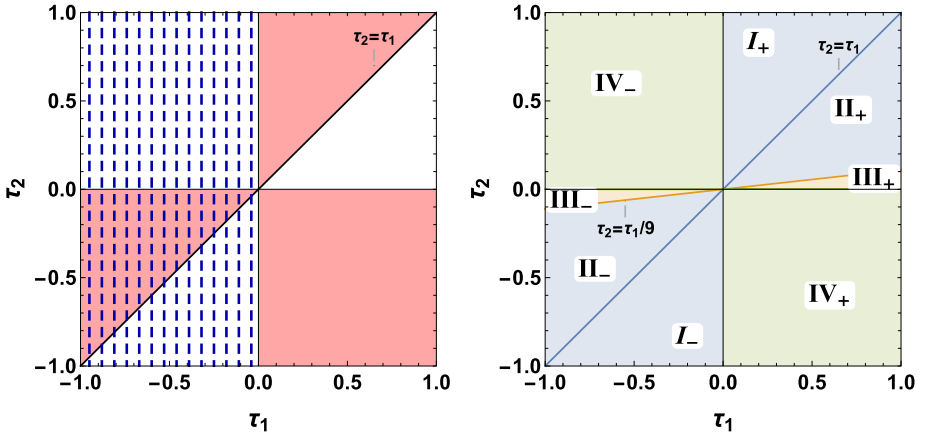

Figure 1 *Left*: Parametric regions of the misbalance timescales τ_1 and τ_2 (Equations 2 and 3) showing amplification of slow MA waves (*red shading*, imaginary parts of two out of three roots (Equation 12) are negative regardless of the sign of the other root for all n) and entropy wave (*blue-dashed lines*, imaginary part of one out of three roots (Equation 12) is negative regardless of the sign of the other two roots for all n). The amplification/attenuation of slow MA and entropy waves corresponds to the regimes of their instability/stability, respectively. *Right*: Parametric regions of τ_1 and τ_2 showing different behaviour of slow MA and entropy waves prescribed by the sign of the discriminant Δ (Equation 11). The *blue-shaded regions* correspond to $\Delta < 0$ for all harmonics n (two propagating slow MA modes and one non-propagating entropy mode, see *Case 1* in Section 3.1). The *green-* and *yellow-shaded regions* show the regimes in which the discriminant Δ can be both positive and negative depending on the harmonic number n (see Table 1). In this case, all three modes become non-propagating for $\Delta > 0$ in a certain range of harmonic numbers n (see *Case 2* in Section 3.1). The Roman numerals indicate specific regions of $\tau_{1,2}$ with different scenarios of the evolution of the entropy and slow MA waves, described in detail in Section 3.2 and demonstrated in Section 5.1. We also recall that the *blue* ($\tau_2 = \tau_1$) and *yellow* ($\tau_2 = \tau_1/9$) *lines* are equivalent to $\gamma_Q = \gamma$ and $\gamma_Q = \gamma/9$, respectively, see Equations 1 – 3. In both panels, the misbalance timescales $\tau_{1,2}$ are normalised to the isothermal acoustic travel time along the loop: L/c_{S0} (see Section 2).

slow MA roots for all harmonic numbers n. This condition is satisfied for

$$\tau_1 < 0, \tag{16}$$

which corresponds to the isobaric instability (see Field, 1965). The same condition for the instability of the entropy mode was used by Kolotkov, Duckenfield, and Nakariakov (2020), in the context of the stability of the solar corona and seismological constraining the coronal-heating function.

In order to determine where in the spectrum (i.e. a specific range of the perturbation harmonic numbers n and the corresponding wavenumbers k) switching between *Cases 1* and *2* takes place, we solve $\Delta = 0$ (Equation 11) with respect to k^2. This gives us three critical wavenumbers: $k_{\rm cr0}$, $k_{\rm cr1}$, and $k_{\rm cr2}$. One of these critical wavenumbers is equal to 0 (i.e. $k_{\rm cr0} = 0$ and $n_{\rm cr0} = 0$), thus corresponding to the non-oscillatory background (see Section 3.1). The other two critical wavenumbers are

$$k_{\rm cr1,2} = \sqrt{\frac{\nu_2^2}{8\gamma^3}\left[\left(\gamma^2 + 18\gamma\gamma_Q - 27\gamma_Q^2\right) \pm \left(\gamma_Q - \gamma\right)^{\frac{1}{2}}\left(9\gamma_Q - \gamma\right)^{\frac{3}{2}}\right]}. \tag{17}$$

Table 1 Relationship between the discriminant sign $\Delta \lessgtr 0$ and the harmonic number n in different parametric regions of the characteristic times τ_1 and τ_2, shown in Figure 1. Negative discriminant $\Delta < 0$ indicates the regime of two propagating and one non-propagating modes (see *Case 1* in Section 3.1). For positive discriminant $\Delta > 0$, all modes become non-propagating (see *Case 2* in Section 3.1). The critical harmonic numbers $n_{\rm cr1}$ and $n_{\rm cr2}$, determining the switch between those regimes, are given in Equation 18.

Regions $I_{\pm}$, $II_{\pm}$ $n_{\rm cr1,2}$ are complex (see blue in Figure 1)	$\Delta < 0$ for all n		
Regions $III_{\pm}$ $n_{\rm cr1,2}$ are real (see yellow in Figure 1)	if $n_{\rm cr1} > n_{\rm cr2} \geq 1$: $\Delta < 0$, $1 \leq n \leq n_{\rm cr2}$ $\Delta > 0$, $n_{\rm cr2}+1 \leq n \leq n_{\rm cr1}$ $\Delta < 0$, $n > n_{\rm cr1}$	if $n_{\rm cr1} \geq 1$, $n_{\rm cr2} = 0$: $\Delta > 0$, $1 \leq n \leq n_{\rm cr1}$ $\Delta < 0$, $n > n_{\rm cr1}$	if $n_{\rm cr1} = n_{\rm cr2} = 0$: $\Delta < 0$ for all n
Regions $IV_{\pm}$ $n_{\rm cr1}$ is real $n_{\rm cr2}$ is complex (see green in Figure 1)	if $n_{\rm cr1} \geq 1$: $\Delta > 0$, $1 \leq n \leq n_{\rm cr1}$ $\Delta < 0$, $n > n_{\rm cr1}$	if $n_{\rm cr1} = 0$: $\Delta < 0$ for all n	

These eigenvalues, in turn, give the critical harmonic numbers at which the change of the discriminant sign happens,

$$n_{\rm cr1} = \text{floor}\left(\frac{k_{\rm cr1}}{\pi} l\right), \quad n_{\rm cr2} = \text{floor}\left(\frac{k_{\rm cr2}}{\pi} l\right). \tag{18}$$

It is clearly seen that the critical harmonic numbers $n_{\rm cr1}$ and $n_{\rm cr2}$ depend on the absolute value and ratio of the characteristic timescales τ_1 and τ_2. These numbers can be either real or complex defining the boundaries of the non-propagating harmonic range (if $n_{\rm cr1}$, $n_{\rm cr2}$ are real, then $n_{\rm cr1} > n_{\rm cr2}$). Thus, the parametric regions of $\tau_{1,2}$ with different sign of the discriminant Δ (Equation 11) across the perturbation spectrum are shown in the right-hand panel of Figure 1. The blue-shaded regions in Figure 1 indicate the regime with $\Delta < 0$ for all harmonic numbers n. It means that *Case 1* holds true for any harmonic in the spectrum, i.e. all slow MA harmonics propagate (see also Table 1). The yellow shading in Figure 1 indicates the region where the discriminant may be either positive or negative. This implies that in some range of the harmonic number n the slow modes become non-propagating (*Case 2*). This range is determined by the critical harmonic numbers $n_{\rm cr1}$ and $n_{\rm cr2}$ (Equation 18). Depending on the absolute value of the characteristic times $\tau_{1,2}$, it may be located at high or low harmonic numbers n and include numerous harmonics (see Table 1). For a particular case with $n_{\rm cr2} = 0$, this range starts from the fundamental harmonic $n = 1$, which thus becomes non-propagating. The green shading in Figure 1 indicates the region where the discriminant may be either positive or negative too. However, in this case the range of non-propagating slow MA harmonics (*Case 2*) may only start from the fundamental harmonic $n = 1$ ($n_{\rm cr2}$ is complex) and is limited by $n_{\rm cr1}$. For $n_{\rm cr1} = n_{\rm cr2} = 0$ in the yellow-shaded regions and for $n_{\rm cr1} = 0$ in the green-shaded regions in Figure 1, *Case 2* degenerates to *Case 1*, i.e. all slow MA harmonics propagate.

In summary, the solution of Equation 9 gives us temporal dependence [$\psi(t)$] of the full solution [$\rho(z,t)$] of the wave Equation 5. It may have two different forms, referred to as *Cases 1* and *2* in this section. The difference is caused by the fact that slow MA harmonics may become non-propagating in a certain range of the perturbation spectrum depending on the characteristic thermal-misbalance timescales $\tau_{1,2}$. The range of non-propagating harmonics may be located at different parts of the spectrum (i.e. at high or low harmonic numbers), and it determined by the critical harmonic numbers [$n_{\rm cr1}$ and $n_{\rm cr2}$] (Equation 18).

The parametric regions of the characteristic times $\tau_{1,2}$ where the change of the solution form takes place are demonstrated in Figure 1 and Table 1. In addition to the effect of non-propagating slow MA harmonics, thermal misbalance leads to the amplification/attenuation of slow MA and entropy modes (see the left-hand panel of Figure 1). Thus, a combination of the left-hand and right-hand panels in Figure 1 should be used for determining values of $\tau_{1,2}$ that allow for i) stable/unstable behaviour of slow MA and entropy waves and ii) propagation/non-propagation of slow MA harmonics. In Section 3.2, we discuss the dependence of the slow MA speed and increments/decrements of slow MA and entropy modes on the harmonic number (i.e. an effective dispersion and frequency-dependent damping/amplification of slow MA and entropy waves, respectively), also caused by the phenomenon of thermal misbalance. A synergy of these effects leads to a number of different scenarios for the initial perturbation to evolve, which are outlined in Section 3.2 and demonstrated in Section 5.1.

3.2. Parametric Regions with Different Behaviour of the Individual Fourier Harmonics

A combination of the left panel (regions of damping/amplification of slow MA and entropy modes) and right panel (regions of propagating/non-propagating slow MA harmonics) in Figure 1 allows us to distinguish parametric regions of $\tau_{1,2}$ with qualitatively different spatio-temporal behaviour of slow MA and entropy waves (the Roman numerals in Figure 1). Quantitatively, the difference in the wave behaviour is caused by the dependence of the phase speed of slow MA waves (the phase speed of the entropy wave is always zero: $\omega_{\mathrm{ER}}/k \equiv 0$) and increment/decrement of slow MA and entropy waves on the harmonic number n (the wavenumber k), which are different for different combinations of the misbalance parameters $\tau_{1,2}$. To illustrate this, we calculated dependencies of the wave increment/decrement and phase speed on the harmonic number n for slow MA and entropy waves in some of those regions (see Figure 2). We used Equations 13 and 14 for the harmonics n satisfying *Case 1*, and general expressions (Equation 12) for the harmonics n satisfying *Case 2*.

As was shown in previous work (e.g. Zavershinskii et al., 2019; Kolotkov, Nakariakov, and Zavershinskii, 2019), the thermal misbalance has a weak impact on the dispersion properties of waves in the short-wavelength limit ($n \to \infty$) and strongly affects them in the long-wavelength limit ($n \to 0$). Assuming that harmonics in both of these limits satisfy *Case 1*, we can write the increments/decrements of entropy and slow MA waves as

$$\lim_{n\to 0} \omega_{\mathrm{EI}} = -\nu_2, \qquad \lim_{n\to \infty} \omega_{\mathrm{EI}} = -\nu_1, \qquad (19)$$

$$\lim_{n\to 0} \omega_{\mathrm{AI}} = 0, \qquad \lim_{n\to \infty} \omega_{\mathrm{AI}} = -\nu_{12},$$

with the parameters ν_1, ν_2, and ν_{12} determined by Equation 6. Equations 19 have no contradiction with the results shown in Figure 1, stating that growth/decay of the entropy wave is defined by the sign of the characteristic time ν_1 (τ_1) for all n. For long-wavelength harmonics ($n \to 0$), *Case 1* occurs only if the characteristic times $\nu_{1,2}$ ($\tau_{1,2}$) are of the same sign (see the first to third rows in Figure 2). Thus, the negative/positive ν_2 (τ_2) is equivalent to the negative/positive ν_1 (τ_1) in this case.

Due to the effect of non-propagation, the slow MA phase speed may have two values in the long-wavelength (strong misbalance) limit:

$$\lim_{n\to 0} \frac{\omega_{\mathrm{AR}}}{k} = c_{\mathrm{SQ}}, \qquad \text{for propagating slow MA waves, } \textit{Case 1} \qquad (20)$$

$$\lim_{n\to 0}\frac{\omega_{\rm AR}}{k}=0, \qquad \text{for non-propagating slow MA waves, } \textit{Case 2}$$

as shown by the first to third rows and the fourth row in Figure 2, respectively. In the short-wavelength limit (weak misbalance), the effect of non-propagation never takes place and slow MA phase speed is not affected by the misbalance process, so that

$$\lim_{n\to\infty}\frac{\omega_{\rm AR}}{k}=c_{\rm S}. \tag{21}$$

Entropy mode in Regions $I_{\pm}-IV_{\pm}$. As shown by Figure 2, in all Regions I_+ to IV_+ the entropy mode decays ($\omega_{\rm EI}<0$). Being excited simultaneously with slow MA modes, the entropy mode contains a part of the initial perturbation energy. Thus, after the slow MA waves run away from the site of the initial perturbation, the essentially non-propagating entropy mode forms a localised density and temperature disturbance that decay with time. However, the decay rate of the individual entropy harmonics is different in those regions. Namely, in Regions I_+ and IV_+ (II_+ and III_+) the shorter- (longer-) wavelength harmonics decay more efficiently, respectively. The situation is symmetrically opposite in Regions I_- to IV_-, where $\omega_{\rm EI}>0$ and the entropy mode grows (not shown in Figure 2).

Slow MA modes in Region I_+. According to the top row in Figure 2, slow MA waves propagate and amplify in Region I_+ ($\omega_{\rm AI}>0$), with higher growth rate at shorter-wavelength harmonics. In this region also, the phase speed of slow MA modes experiences a negative dispersion, i.e. longer-wavelength harmonics propagate faster than those with shorter-wavelength. A combination of these effects leads to the formation of propagating quasi-periodic patterns, which could be referred to as slow MA wave trains. The linear stage of their formation (with the relative amplitude of the plasma density perturbation $\rho\ll 1$) from the initial Gaussian pulse has been discussed in detail by Zavershinskii et al. (2019) in terms of the linear Equation 5. In a weakly nonlinear regime with $\rho\lessapprox 1$, the growing slow MA wave develops into self-sustained shock pulses, for description of which a nonlinear evolutionary equation is required (see, e.g., Molevich et al., 2011; Zavershinskii et al., 2020). The strong amplification may also lead to highly nonlinear variations with $\rho\gtrsim 1$. In this case, parameters of the nonlinear slow MA shock structures can be found using the solution of the full set of hydrodynamic equations (Molevich and Ryashchikov, 2020).

Slow MA modes in Region II_+. The second row of Figure 2 shows properties of slow MA modes in Region II_+. In this case, slow MA waves propagate and decay ($\omega_{\rm AI}<0$) with larger decrease for shorter-wavelength harmonics. The phase speed of slow MA modes has a positive dispersion, with shorter-wavelength harmonics overtaking. In this case, the effect of dispersion and frequency-dependent damping causes the initial Gaussian pulse to become asymmetric, broaden, and decrease in its amplitude with time (see Zavershinskii et al., 2019, for details). As both slow MA waves decay in this case, the description of nonlinear effects is required only in the case of a nonlinear initial perturbation.

Slow MA modes in Region III_+. In this region of the misbalance parameters $\tau_{1,2}$ (see the third row of Figure 2), the range of non-propagating slow MA harmonics may appear in the spectrum (see *Case 2* in Section 3.1), that is determined by the critical wavenumbers $n_{\rm cr1}$ and $n_{\rm cr2}$ (Equation 18). Both the propagating slow MA waves with $\omega_{\rm AI}<0$ and all non-propagating harmonics with purely imaginary $\omega_{1,2,3}<0$ decay in this region. The dispersion of the phase speed can be either positive or negative in this region. For harmonics $n<n_{\rm cr2}$, the dispersion is negative and $|\omega_{\rm AI}|$ is lower (weaker damping); for harmonics $n>n_{\rm cr1}$, it becomes positive and $|\omega_{\rm AI}|$ is higher (stronger damping). Potentially, formation of quasi-periodic slow MA structures from a broadband initial perturbation due to the negative dispersion and weak damping in the long-wavelength band is possible. However, the effect is

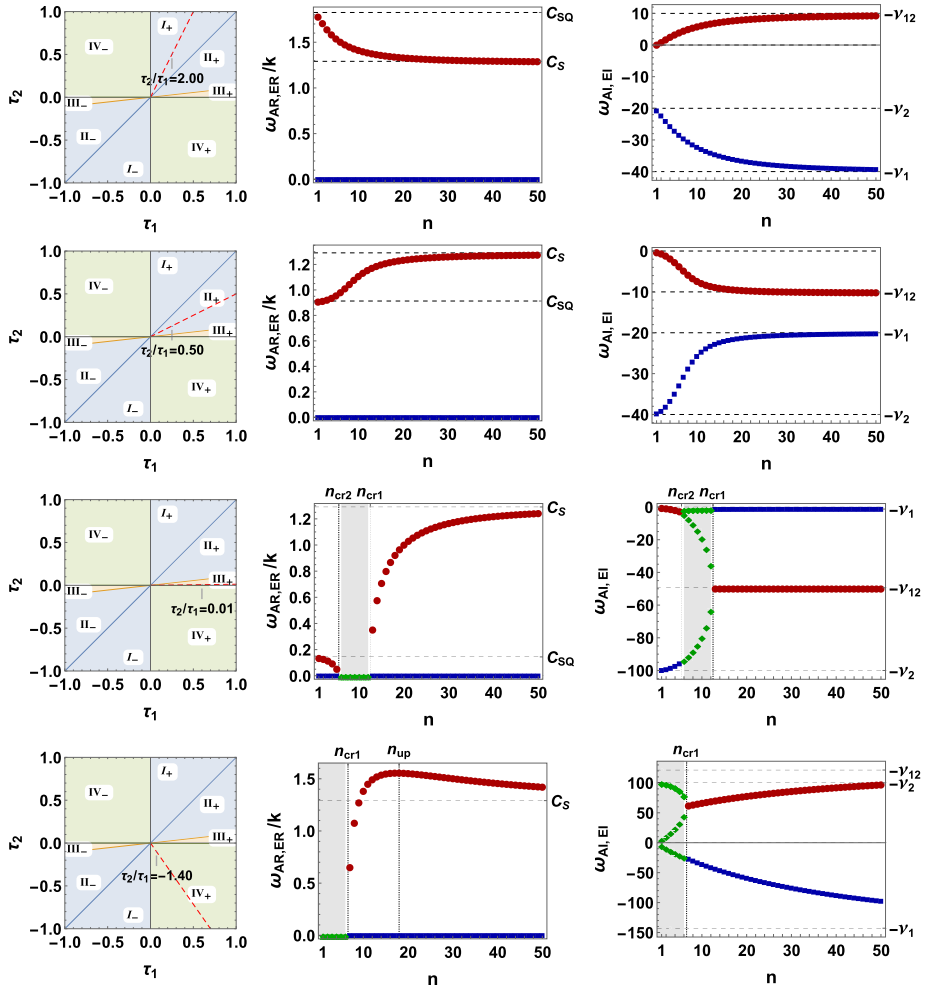

Figure 2 *Left column* indicates the regions of the thermal-misbalance timescales $[\tau_{1,2}]$ in which the dispersive properties of slow MA and entropy waves are qualitatively different (see also Figure 1), with $\tau_2/\tau_1 = 2$ in Region I_+ (the *top row*), $\tau_2/\tau_1 = 0.5$ in Region II_+ (the *second row*), $\tau_2/\tau_1 = 0.01$ in Region III_+ (the *third row*), and $\tau_2/\tau_1 = -1.4$ in Region IV_+ (the *bottom row*). *Middle and right columns* show the dependence of the phase speed $\omega_{\rm AR,ER}/k$ and increment/decrement $\omega_{\rm AI,EI}$ of the slow MA and entropy modes on the harmonic number n, respectively. The dependencies are calculated using Equations 13 and 14 for harmonics n satisfying *Case 1*, and general expressions (Equation 12) for harmonics n satisfying *Case 2*. The *red symbols* correspond to the harmonics of two propagating slow MA waves. The *blue symbols* correspond to the entropy mode. The *green symbols* correspond to the harmonics satisfying *Case 2*, for which all three modes become non-propagating. The ranges of n in which those non-propagating slow MA harmonics appear are determined by the critical harmonic numbers $n_{\rm cr1,2}$ (Equation 18) and shown by grey shading. The harmonic number $n_{\rm up}$ shows the change of the sign of the gradient of the dependence $\omega_{\rm AR}(n)$ in Region IV_+, and is obtained from the condition $\partial\omega_{\rm AR}/\partial n = 0$. The limiting values of the slow MA phase speed $[c_{\rm S}$ and $c_{{\rm S}Q}]$ are given in Equation 1, and normalised to the isothermal sound speed $c_{\rm S0}$. The limiting values of the slow MA and entropy increments/decrements, $\nu_{1,2}$ and ν_{12} are given by Equation 6.

Table 2 Exact solution of Equation 5 in different regions of the characteristic thermal-misbalance timescales $\tau_{1,2}$ (see Figure 1), for $n_{\rm cr1} > n_{\rm cr2} > 1$ (Equation 18). The functions $\rho_{n\Delta-}(z,t)$, $\rho_{n\Delta+}(z,t)$, and $\rho_0(z,t)$ are given in Equations 22, 28, and 30, respectively.

Region	Solution
$I_\pm$, $II_\pm$	$\rho(z,t) = \rho_0(z,t) + \sum_{n=1}^{\infty} \rho_{n\Delta-}(z,t)$
$III_\pm$	$\rho(z,t) = \rho_0(z,t) + \sum_{n=1}^{n_{\rm cr2}} \rho_{n\Delta-}(z,t) + \sum_{n=n_{\rm cr2}+1}^{n_{\rm cr1}} \rho_{n\Delta+}(z,t) + \sum_{n=n_{\rm cr1}+1}^{\infty} \rho_{n\Delta-}(z,t)$
$IV_\pm$	$\rho(z,t) = \rho_0(z,t) + \sum_{n=1}^{n_{\rm cr1}} \rho_{n\Delta+}(z,t) + \sum_{n=n_{\rm cr1}+1}^{\infty} \rho_{n\Delta-}(z,t)$

likely to be less pronounced than in Region I_+ due to a small number of harmonics $n < n_{cr2}$, and relatively low variation of their phase speed between c_{SQ} and 0. Indeed, in this region, the maximum value of c_{SQ} prescribed by $\gamma_Q = \gamma\tau_2/\tau_1$ is $c_S/3$ that is associated with the upper boundary of Region III_+, $0 < \tau_2/\tau_1 < 1/9$.

Slow MA modes in Region IV_+. In this region (see the bottom row in Figure 2), the range of non-propagating slow MA harmonics may also appear in the spectrum. However, in contrast to Region III_+, slow MA waves grow with $\omega_{\rm AI} > 0$. Similarly to Region III_+, the non-propagating slow MA harmonics may have both higher and lower increments relative to the propagating harmonics. The phase speed of slow MA waves is a non-monotonic function of the harmonic number n, providing either positive or negative dispersion (see the middle panel in the bottom row of Figure 2). The range of propagating harmonics with positive dispersion has a finite number of harmonics. The lower limit of this range is determined by the critical number $n_{\rm cr1}$ (Equation 18). The upper limit, $n_{\rm up}$ can be found by solving the equation $\partial\omega_{\rm AR}/\partial n = 0$ (Equation 14). The range of harmonics with negative dispersion, in turn, has no upper limit. A combination of negative dispersion and amplification again may lead to formation of quasi-periodic slow MA patterns. The effect will be more strongly pronounced for low values of $n_{\rm up}$, so that the majority of slow MA harmonics will have negative dispersion. The dispersion properties of slow MA waves in this case will be qualitatively similar to those in Region I_+. The amplifying non-propagating slow MA harmonics in Region IV_+, which occur for the harmonic numbers $1 < n < n_{\rm cr1}$, would develop into long-wavelength density disturbances, similarly to those caused by the entropy mode, thus making the plasma essentially non-uniform along the field.

In Regions I_- to IV_-, the properties of slow MA waves are symmetrically opposite to those in Regions I_+ to IV_+ described above. Hence, these regions are not shown in Figure 2.

Thus, the dispersive properties of slow MA and entropy waves are shown to strongly depend on the characteristic timescales τ_1 and τ_2 of the thermal-misbalance process, that may lead to dramatically different scenarios for the evolution of the initial broadband perturbation of the coronal plasma. For illustration, in Section 5 we show how entropy and slow MA modes excited simultaneously share the initial perturbation energy and evolve in the linear regime in Regions $I_\pm$ and $II_\pm$, using the exact full solution $\rho(z,t)$ presented in Section 4.

4. Exact Solution

In Section 3, we have discussed the spatial $\varphi(z)$ and temporal $\psi(t)$ dependencies of the full solution $\rho(z,t) = \varphi(z)\,\psi(t)$, described by Equations 7 and 9, respectively. Using solutions

to these equations, in this section we present the full exact solution of the governing evolutionary Equation 5 for the density perturbation $\rho(z,t)$ caused by a superposition of slow MA and entropy waves with harmonic number n. There are three possible cases:

i) The solution for the nth harmonic with $\Delta < 0$ (*Case 1*: two oppositely propagating slow MA modes and one non-propagating entropy mode),

$$\rho_{n\Delta-}(z,t) = C_{1n}\mathrm{e}^{\omega_{\mathrm{EI}}t}\cos(kz) + C_{0n}\mathrm{e}^{\omega_{\mathrm{AI}}t}\left[\cos(\omega_{\mathrm{AR}}t + kz - \phi_n) + \cos(\omega_{\mathrm{AR}}t - kz - \phi_n)\right], \tag{22}$$

where

$$C_{0n} = \frac{\sqrt{C_{2n}^2 + C_{3n}^2}}{2}, \quad \phi_n = \arctan\left(\frac{C_{3n}}{C_{2n}}\right). \tag{23}$$

The constants C_{1n}, C_{2n}, and C_{3n} can be obtained by solving the following set of linear equations:

$$\begin{pmatrix} 1 & 1 & 0 \\ \omega_{\mathrm{EI}} & -\omega_{\mathrm{AI}} & \omega_{\mathrm{AR}} \\ \omega_{\mathrm{EI}}^2 & \left(\omega_{\mathrm{AI}}^2 - \omega_{\mathrm{AR}}^2\right) & -2\omega_{\mathrm{AR}}\omega_{\mathrm{AI}} \end{pmatrix} \begin{pmatrix} C_{1n} \\ C_{2n} \\ C_{3n} \end{pmatrix} = \begin{pmatrix} I_{1n} \\ I_{2n} \\ I_{3n} \end{pmatrix}. \tag{24}$$

The integrals I_{1n}, I_{2n}, and I_{3n} are prescribed by the initial perturbation $\rho_{\mathrm{in}}(z,0)$ and the derivatives $(\partial\rho(z,t)/\partial t)|_{t=0}$, and $(\partial^2\rho(z,t)/\partial t^2)\big|_{t=0}$ as

$$I_{1n} = \frac{2}{l}\int_0^l \rho_{\mathrm{in}}(z,0)\cos(kz)\,\mathrm{d}z, \tag{25}$$

$$I_{2n} = \frac{2}{l}\int_0^l \left.\frac{\partial\rho(z,t)}{\partial t}\right|_{t=0}\cos(kz)\,\mathrm{d}z, \tag{26}$$

$$I_{3n} = \frac{2}{l}\int_0^l \left.\frac{\partial^2\rho(z,t)}{\partial t^2}\right|_{t=0}\cos(kz)\,\mathrm{d}z. \tag{27}$$

ii) The solution for the nth harmonic with $\Delta > 0$ (*Case 2*: all three modes non-propagating),

$$\rho_{n\Delta+}(z,t) = \left(C_{1n}\mathrm{e}^{-\mathrm{i}\omega_1 t} + C_{2n}\mathrm{e}^{-\mathrm{i}\omega_2 t} + C_{3n}\mathrm{e}^{-\mathrm{i}\omega_3 t}\right)\cos(kz). \tag{28}$$

The constants C_{1n}, C_{2n}, and C_{3n} can be obtained by solving the following set of linear equations:

$$\begin{pmatrix} 1 & 1 & 1 \\ \omega_1 & \omega_2 & \omega_3 \\ \omega_1^2 & \omega_2^2 & \omega_3^2 \end{pmatrix} \begin{pmatrix} C_{1n} \\ C_{2n} \\ C_{3n} \end{pmatrix} = \begin{pmatrix} I_{1n} \\ I_{2n} \\ I_{3n} \end{pmatrix}, \tag{29}$$

with the integrals I_{1n}, I_{2n}, and I_{3n} determined by Equations 25 – 27.

iii) A non-oscillating and non-propagating background value with $\Delta = 0$ and $n = 0$ is

$$\rho_0(z,t) = C_{10}\mathrm{e}^{-\nu_2 t} + C_{20}t + C_{30}. \tag{30}$$

The constants C_{10}, C_{20}, and C_{30} can be obtained by solving the following set of linear equations:

$$\begin{pmatrix} 1 & 0 & 1 \\ -\nu_2 & 1 & 0 \\ \nu_2^2 & 0 & 0 \end{pmatrix} \begin{pmatrix} C_{10} \\ C_{20} \\ C_{30} \end{pmatrix} = \begin{pmatrix} I_{10} \\ I_{20} \\ I_{30} \end{pmatrix}, \tag{31}$$

where

$$I_{10} = \frac{1}{l} \int_0^l \rho_{\rm in}(z,0) \mathrm{d}z, \tag{32}$$

$$I_{20} = \frac{1}{l} \int_0^l \left. \frac{\partial \rho(z,t)}{\partial t} \right|_{t=0} \mathrm{d}z, \tag{33}$$

$$I_{30} = \frac{1}{l} \int_0^l \left. \frac{\partial^2 \rho(z,t)}{\partial t^2} \right|_{t=0} \mathrm{d}z. \tag{34}$$

Using Equations 22, 28, and 30, we can construct the exact solution of Equation 5 by the superposition principle. In other words, to obtain the exact solution we sum up the solutions for all harmonics from $n = 1$ to infinity, using Equations 22 and 28 for harmonics satisfying $\Delta < 0$ and $\Delta > 0$, respectively, and add Equation 30 for a non-oscillating background ($n = 0$). The series describing the exact solution for different regions of the characteristic thermal-misbalance timescales $\tau_{1,2}$ (see Figure 1) are presented in Table 2. The exact solution obtained gives us plenty of possibilities for the analysis of the perturbation evolution.

5. Applications of the Exact Solution

The exact solution shown in Table 2, in particular, allows us to study the initial (linear) stage of the perturbation evolution in any regions of the characteristic misbalance times [τ_1 and τ_2]. Moreover, it allows us to study the evolution of slow MA and entropy waves separately, attributing the first and second terms on the RHS of Equation 22 to the entropy and slow MA mode, respectively. As was discussed in Section 3, this distinct attribution is only possible for *Case 1* with the discriminant $\Delta < 0$ (Equation 11), while in *Case 2* with $\Delta > 0$ and the solution of Equation 28 it is less obvious because of the mixed properties of those waves. Hence, in this section, for illustration we apply the obtained exact solution to the evolution of the initial localised perturbation in parametric Regions $I_{\pm}$ and $II_{\pm}$ (see Figure 1), throughout which *Case 1* holds true, i.e. all slow MA harmonics propagate and all entropy harmonics do not propagate.

5.1. Spatio-Temporal Evolution of Entropy and Slow MA Modes

The specific form of the initial perturbation is determined by its functional dependence on the z-coordinate and what plasma parameters are perturbed. This in turn determines the functions $\rho_{in}(z,0)$, $(\partial\rho(z,t)/\partial t)|_{t=0}$, and $(\partial^2\rho(z,t)/\partial t^2)\big|_{t=0}$, which affect the partition of the initial perturbation energy between slow MA and entropy waves, according to Equation 24. From the set of governing MHD equations written for the perturbations along the field in a zero-β plasma (see, e.g., Equations 1 – 4 of Zavershinskii et al., 2019), the derivatives $\partial\rho(z,t)/\partial t$ and $\partial^2\rho(z,t)/\partial t^2$ (and hence their values at $t = 0$) are connected with the

perturbations of the other plasma parameters as

$$\frac{\partial \rho(z,t)}{\partial t} = -\frac{\partial V_z(z,t)}{\partial z}, \tag{35}$$

$$\frac{\partial^2 \rho(z,t)}{\partial t^2} = \frac{\partial^2 P(z,t)}{\partial z^2}. \tag{36}$$

In this work, we consider an initial Gaussian pulse perturbing the plasma density, pressure, and temperature,

$$\begin{aligned} \rho_{\rm in}(z,0) &= A_\rho \exp\left[-(z-z_0)^2/w\right], \\ P_{\rm in}(z,0) &= A_P \exp\left[-(z-z_0)^2/w\right], \\ T_{\rm in}(z,0) &= P_{\rm in}(z,0) - \rho_{\rm in}(z,0), \\ V_{z,\rm in}(z,0) &= 0. \end{aligned} \tag{37}$$

Here, the initial perturbation of the plasma velocity $V_{z,\rm in}$ is taken to be zero, implying the absence of the injected plasma flows. All the initial perturbations (Equation 37) are normalised to the equilibrium values ρ_0, $\rho_0 c_{\rm S0}^2$, T_0, and $c_{\rm S0}$, respectively; A_ρ and A_P are magnitudes of the density and pressure variations; w and z_0 are the effective width and position of the perturbing pulse, respectively. We assume here that $A_\rho = A_P$, which implies that the initial perturbation (Equation 37) is of an isothermal type (i.e. $T_{\rm in} = 0$). This assumption is justified, for example, for perturbations by impulsive heating events in the solar corona, in which the rapid increase in the plasma temperature strengthens the efficiency of the parallel thermal conduction that tends to smooth the temperature perturbation out, on a timescale much shorter than the timescale of the waves excited (see, e.g., Reale, 2016; Reale et al., 2018, 2019). In addition, it can be shown that, for the initial perturbation (Equation 37), the coefficients C_{10} and C_{20} in Equation 30 are equal to zero, so that the background value $[\rho_0]$ does not vary in time and, hence, does not affect the damping or amplification of entropy and slow MA modes.

In the examples shown in Figure 3, we focus on the evolution of the entropy wave and one slow MA wave, as the evolution of the other slow MA wave is symmetrical. Thus, for demonstration of the solution at $t = 0$ we use half of the second term in Equation 22. For $t \neq 0$, the second slow MA wave escapes the z-domain shown in Figure 3 and is therefore not visible. We have varied the width $[w]$ of the initial signal (Equation 37) to obtain the most illustrative examples.

In the top row of Figure 3, we show evolution of the isothermal density perturbation (Equation 37) in Region I_+ of the characteristic thermal-misbalance times $\tau_{1,2}$, shown in Figure 1. As was demonstrated in Section 3, the entropy mode attenuates in this region of parameters. The slow MA mode, in turn, forms a propagating quasi-periodic pattern at some distance from the site of the initial perturbation with the characteristic wavelength about $0.1L$ and period about $0.07L/c_{\rm S0}$, as a result of amplification of its harmonics and negative dispersion of the phase speed (see the top row of panels in Figure 2 and discussion in Section 3.2). For example, for typical parameters of coronal loops with $L = 200$ Mm and $T_0 = 1-10$ MK, the wavelength and period are 20 Mm and 40 – 120 seconds, respectively. The formation of a similar propagating slow MA wave train for a set of parameters from Region I_+ was demonstrated by Zavershinskii et al. (2019) by numerical solution of the evolutionary Equation 5, i.e. without separating the total solution into the individual entropy and slow MA waves.

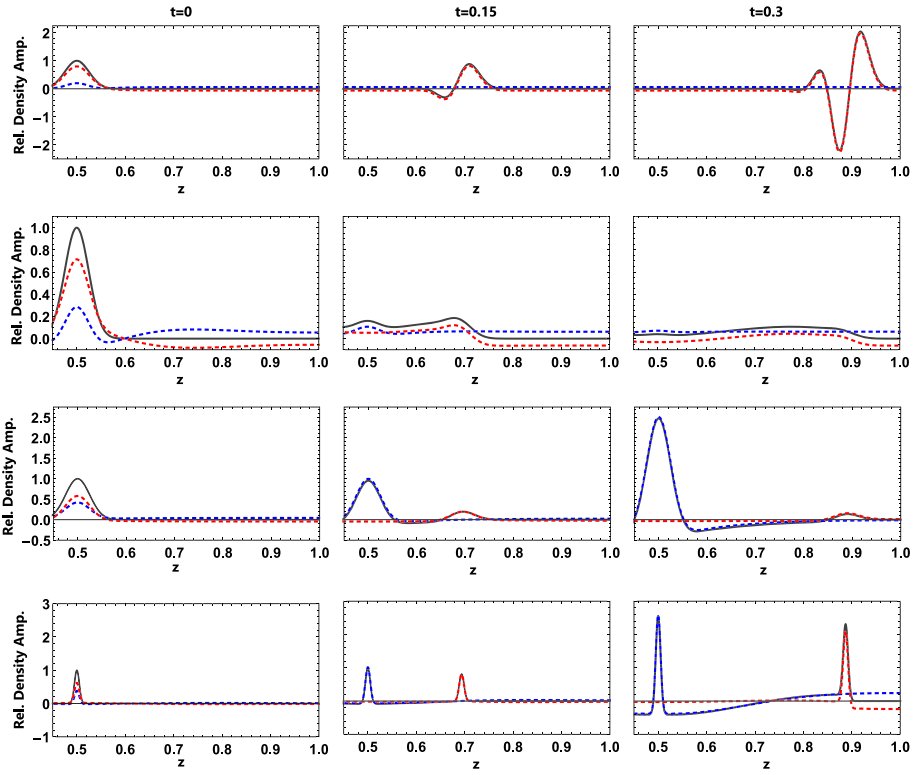

Figure 3 Evolution of the initial plasma-density perturbation of a Gaussian shape (Equation 37) situated at $z_0 = l/2$, in the parametric Regions I_+ with $\tau_2 = 0.016$ and $\tau_1 = 0.01$ (*top row*); II_+ with $\tau_2 = 0.04$ and $\tau_1 = 0.1$ (*second row*); I_- with $\tau_2 = -0.4$ and $\tau_1 = -0.15$ (*third row*); and II_- with $\tau_2 = -0.05$ and $\tau_1 = -0.15$ (*bottom row*) of the characteristic misbalance timescales $\tau_{1,2}$ (see Figure 1). The exact analytical solution describing the wave evolution in those regions is given in Table 2. *Left*, *middle*, and *right* columns indicate the solutions at $t = 0$, $t = 0.15$, and $t = 0.3$ of the computational time, respectively. The *red* and *blue dashed lines* correspond to one slow MA mode and one entropy mode, respectively. The *solid black line* corresponds to the full solution (sum of solutions for one entropy and two slow MA modes). The relative-density amplitude on the *vertical axis* is shown in the units of the initial density pulse amplitude $[A_\rho]$, shared between one entropy wave and two slow MA waves. The *horizontal axis* is normalised to the characteristic spatial scale of the medium (for example, the loop length $[L]$). The background value $[\rho_0(z,t)]$ (see Table 2) is included into the entropy-mode solution (the *blue lines*), since it does not propagate (similarly to all harmonics of the entropy wave.) Animations showing the evolution of separate modes and the development of full density perturbation (sum of entropy and slow MA modes) can be found in the Supplementary Materials.

The second row in Figure 3 was obtained for a set of parameters $\tau_{1,2}$ corresponding to Region II_+ in Figure 1 and the second row of panels in Figure 2. In this case, both the entropy and the slow MA waves decay, leading to the disappearance of the density perturbation. Moreover, the decaying and propagating slow MA pulse becomes strongly asymmetric. This effect is caused by a positive dispersion of the slow MA phase speed accompanied by stronger damping of higher harmonics. In addition, the slow MA pulse shape is affected by the effective excitation of the entropy mode in such a thermodynamically active plasma that violates the symmetry in the partition of the initial perturbation energy across the spectrum.

The decay of the propagating slow MA pulse in this regime was also shown numerically by Zavershinskii et al. (2019), without discussion of the entropy-mode behaviour.

The wave evolution in Region I_- of the parameters $\tau_{1,2}$ is shown by the third row of Figure 3. In this case, the entropy mode grows and leads to the formation of a localised plasma condensation at the site of the initial perturbation. The slow MA mode, in turn, runs away from the perturbation epicenter and decays. In the coronal context, for example, this regime could correspond to observations or numerical simulations of coronal rain formed in response to impulsive perturbations of the coronal mechanical and thermal equilibria, with weakly pronounced (or not pronounced at all) signatures of slow MA waves (see, e.g., Kohutova et al., 2020).

The opposite situation occurs in Region II_- (see the bottom row in Figure 3), in which both entropy and slow MA modes are amplified. Thus, one should expect to observe an effective formation of localised plasma condensations by the growing entropy mode, accompanied by well developed and visible propagating slow MA waves. The exponential growth of both modes in this regime will breach the realm of the linear analysis when the perturbation amplitude becomes sufficiently large. However, taking additional dissipative processes, such as thermal conduction and viscosity, into account may suppress the wave growth rates or even stabilise the perturbations, thus extending the range of applicability of the developed linear theory. This issue will be addressed in follow-up work.

5.2. Partition of Energy between Entropy and Slow MA Modes

In this section, we consider the question of the relative efficiency of the excitation of slow MA and entropy waves in a plasma with heating/cooling misbalance. The set of linear equations (Equation 24) connecting the initial amplitude coefficients [C_{1n}, C_{2n}, and C_{3n}] of the entropy and slow MA waves with the initial perturbation [$\rho_{in}(z,0)$, $(\partial\rho(z,t)/\partial t)|_{t=0}$, and $(\partial^2\rho(z,t)/\partial t^2)\big|_{t=0}$] can be treated as effective initial Fourier spectra of those waves, providing the distribution of the initial perturbation energy over the harmonic numbers n. Moreover, the partition of this initial energy between the entropy and slow MA waves and their harmonics is seen to directly depend on the properties of the plasma heat-loss function $Q(\rho, T)$ through the presence of the parameters $\tau_{1,2}$ on the LHS of Equation 24. In other words, for some regimes of the misbalance (values of $\tau_{1,2}$) the entropy/slow MA waves could be excited with a higher/lower efficiency. We also note that the question of this energy partition makes sense only for the regimes of decaying waves, as otherwise the wave instability would cause the amplitude to grow exponentially independently of its initial value. Hence, in this section we consider Region II_+ of the misbalance parameters $\tau_{1,2}$ (see Figure 1), for which both modes decay and all slow MA harmonics propagate.

In this work, we do not discuss the distribution of the initial energy over the individual entropy and slow MA harmonics, but focus on the partition of the total (i.e. integrated over all harmonics) initial energy between the modes. Thus, the ratio of the total initial energies $\mathcal{E}_{\rm tot}$ and $\mathcal{A}_{\rm tot}$ gained by the entropy and slow MA modes, respectively, from the initial Gaussian pulse (Equation 37) can be estimated as

$$\frac{\mathcal{E}_{\rm tot}}{\mathcal{A}_{\rm tot}} = \sum_{n=1}^{\infty} C_{1n}^2 / 2 \sum_{n=1}^{\infty} C_{0n}^2, \tag{38}$$

where

$$\mathcal{E}_{\rm tot} = \sum_{n=1}^{\infty} \left[\frac{I_{1n}\left(\omega_{\rm AR}^2 + \omega_{\rm AI}^2\right) + I_{3n}}{\omega_{\rm AR}^2 + \left(\omega_{\rm AI} + \omega_{\rm EI}\right)^2} \right]^2,$$

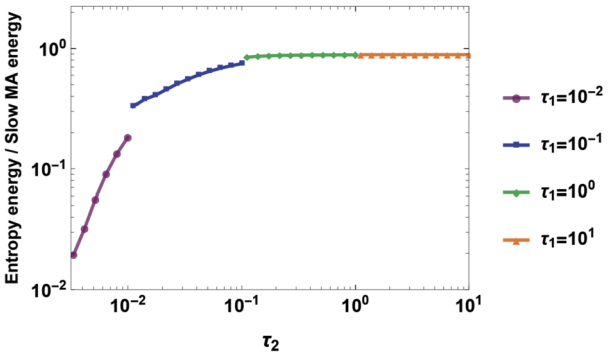

Figure 4 Dependence of ratio $\mathcal{E}_{\rm tot}/\mathcal{A}_{\rm tot}$ (Equation 38) of the entropy-mode energy to slow-mode energy on the misbalance timescale τ_2 calculated for 200 harmonics and for different values of the timescale τ_1 in the parametric Region II_+ (see Figure 1), i.e. $\tau_1/9 \le \tau_2 \le \tau_1$. Both parameters τ_1 and τ_2 are normalised to the isothermal acoustic travel time along the loop $[L/c_{S0}]$.

$$\mathcal{A}_{\rm tot} = \sum_{n=1}^{\infty} \frac{\omega_{\rm EI}^2 I_{1n}^2 \left(\omega_{\rm AR}^2 + \omega_{\rm AI}^2\right) - 2\omega_{\rm EI}\omega_{\rm AI} I_{1n} I_{3n} + I_{3n}^2}{\omega_{\rm AR}^2 \left[\omega_{\rm AR}^2 + (\omega_{\rm AI} + \omega_{\rm EI})^2\right]}.$$

The values of the integrals I_{1n} and I_{3n} can be obtained either analytically or numerically using Equations 25 – 27 for the chosen initial conditions (Equations 35 – 37).

Figure 4 shows the dependence of the entropy to slow MA total energy ratio $[\mathcal{E}_{\rm tot}/\mathcal{A}_{\rm tot}]$ (Equation 38) on the characteristic misbalance times $\tau_{1,2}$. It is seen that, for $\tau_{1,2} \ge 1$ in the considered Region $[II_+]$, the total initial energy of slow MA waves is almost equal to the total initial energy of the entropy wave. For lower values of $\tau_{1,2}$, the ratio $\mathcal{E}_{\rm tot}/\mathcal{A}_{\rm tot}$ decreases, indicating a preferential excitation of slow MA waves in this regime of thermal misbalance.

6. Summary and Conclusions

The exact solution obtained (Table 2) presents the effects of thermal misbalance on the evolution of entropy and slow MA waves in the optically thin, non-adiabatic plasma of the hot solar corona. It gives us comprehensive information about the spatio-temporal dynamics and dispersive properties of those waves, allows for the analysis of the energy partition between slow MA and entropy waves and across their harmonics. In particular, the theory developed here allowed us to identify the regimes in which properties of slow MA and entropy waves get mixed through the mechanism of thermal misbalance. Now we summarise the distinct misbalance-caused features of those waves, which have been revealed using the exact solution obtained.

i) The exact analytical solution of the dispersion relation (Equation 10) of slow MA and entropy waves is obtained without assumption of weak amplification/attenuation (cf. the previous work on thermal misbalance by Zavershinskii et al., 2019; Kolotkov, Nakariakov, and Zavershinskii, 2019; Duckenfield, Kolotkov, and Nakariakov, 2021), where the dispersion relation was solved under this assumptions. It allowed us to obtain the dependence of the phase speed and increment/decrement of entropy and slow MA waves on wavenumbers (see Figure 2). In particular, it is shown that for some regimes of thermal misbalance the dependence of the slow MA wave phase speed on wavenumber can be even non-monotonic (see the third and fourth rows in Figure 2).

ii) The theory presented is developed for any values of the characteristic misbalance timescales $[\tau_{1,2}]$. Indeed, previous estimations of $\tau_{1,2}$ for typical coronal conditions showed that they could be either positive or negative, depending on the specific form of the coronal-heating function (Kolotkov, Duckenfield, and Nakariakov, 2020). Thus,

the quantitative analysis performed in our work generalises and extends the qualitative picture of the impact of thermal misbalance on slow MA and entropy modes shown in Table 2 of Kolotkov, Duckenfield, and Nakariakov (2020).

iii) For specific regimes of thermal misbalance prescribed by the values of its characteristic timescales $\tau_{1,2}$, harmonics of slow MA modes may become non-propagating. The cut-off wavenumbers $k_{\rm cr1}$ and $k_{\rm cr2}$ (Equation 17) defining the non-propagating range have been obtained analytically. In this non-propagating regime, slow MA and entropy harmonics manifest mixed properties, so that the perturbation of a low-β coronal plasma caused by these modes would look identical, as a non-propagating disturbance of the plasma density either growing or decaying with time. The longitudinal structuring of plasma density and temperature in coronal loops that are initially uniform along the field, caused by those non-propagating slow MA harmonics, may have different spatial scales depending on the values of the cut-off wavenumbers [$k_{\rm cr1}$ and $k_{\rm cr2}$]. Traditionally, the parallel non-uniformity of plasma structures in the solar atmosphere, affecting the dynamics of magnetoacoustic waves, is associated with the gravitational density stratification and/or divergence of the magnetic-field lines with height (see, e.g., De Moortel and Hood, 2004; Andries, Arregui, and Goossens, 2005; McEwan et al., 2006; Botha et al., 2011; Luna-Cardozo, Verth, and Erdélyi, 2012; Riedl, Van Doorsselaere, and Santamaria, 2019). In this context, the non-propagation of essentially compressive, slow MA harmonics offers an alternative mechanism for creating non-uniformity of plasma along the loop, leading to the necessity to consider the interaction between the perturbing wave and the non-uniformity of the background plasma caused by this wave, and also indirectly affecting the waves elsewhere in the loop (see, e.g., Nisticò et al., 2017, where the slow and fast kink magnetoacoustic oscillations were observed to co-exist in a bundle of coronal loops). A detailed analysis and validation of this effect and its consequences for coronal MHD seismology would require comprehensive numerical simulations, taking nonlinear and additional dissipative effects into account.

iv) There are a number of different scenarios for the evolution of the initial perturbation caused by the combination of a frequency-dependent damping/amplification of slow MA and entropy modes and monotonic positive/negative or non-monotonic dispersion of slow MA waves, associated with the phenomenon of thermal misbalance. In particular, the entropy wave could decay and slow MA wave grow and develop into a propagating quasi-periodic slow MA wave train; both waves decay smoothing the initial perturbation out; the entropy wave grows and forms a localised condensation of the plasma density, while the slow MA wave runs away and decays; both slow and entropy waves grow. In the regime of formation of slow MA wave trains, their characteristic period for typical coronal conditions is shown to be a few minutes, which coincides with typical periods of quasi-periodic pulsations often observed in the thermal emission from solar flares and usually interpreted in terms of the evolution of compressive MHD waves in the solar atmosphere (see, e.g., Van Doorsselaere, Kupriyanova, and Yuan, 2016; McLaughlin et al., 2018; Kupriyanova et al., 2020). The regime of formation of the localised plasma condensations by the instability of the entropy mode is of a clear importance in the context of coronal-rain formation (see, e.g., Antolin, Shibata, and Vissers, 2010; Fang, Xia, and Keppens, 2013). In particular, the dynamics of a similar localised plasma condensation of an unspecified nature in a gravitationally stratified coronal loop was considered by Kohutova and Verwichte (2017), the initial formation of which could be self-consistently attributed to the instability of the entropy mode through the mechanism of thermal misbalance, developed in our work. The regime of misbalance causing both waves to decay could be used for the interpretation of rapid damping of standing,

propagating, and sloshing slow MA waves in quiescent and active-region coronal loops, polar plumes, and interplume regions (De Moortel, 2009; Wang, 2011; Banerjee, Gupta, and Teriaca, 2011; Nakariakov et al., 2019). The first successful attempts of applying the phenomenon of thermal misbalance to observations of rapidly decaying, standing slow MA oscillations (also known as SUMER oscillations) in hot and dense loops in active regions were performed by Kolotkov, Nakariakov, and Zavershinskii (2019) and Prasad, Srivastava, and Wang (2021).

v) The initial distribution of energy in and between slow MA and entropy waves depends on the properties of the coronal heat-loss function $[Q(\rho, T)]$. It has been shown that for the initial perturbation of an isothermal nature the total initial energies are either equal or most goes into slow MA waves. In particular, for the characteristic misbalance timescales $\tau_{1,2}$ being about the acoustic travel time along the loop and higher, the ratio between the entropy and slow MA wave initial energies is about unity. For lower values of $\tau_{1,2}$, this ratio becomes smaller. The estimation of this energy partition would also depend on the type of the initial perturbation. For example, excitation of slow MA waves in coronal loops by injected flows is often considered in modelling (see, e.g., Ofman, Wang, and Davila, 2012; Wang, Ofman, and Davila, 2013; Provornikova, Ofman, and Wang, 2018), and it could lead to a different dependence of the entropy wave to slow MA wave total initial-energy ratio on the misbalance parameters $\tau_{1,2}$. A more detailed analysis of this question constitutes another potentially important follow-up of this work.

Taking additional dissipative processes such as parallel thermal conduction and compressive viscosity into account in future work would broaden the applicability of the developed theory and obtained exact analytical solution. We expect that those additional dissipative processes of the coronal plasma may change the picture presented in this work quantitatively but not qualitatively, i.e. the aforementioned effects of thermal misbalance on the evolution of slow MA and entropy waves will be retained. We also would like to mention that, similarly to the process of parallel thermal conduction, the phenomenon of thermal misbalance could lead to the appearance of additional phase shifts between slow MA perturbations of the plasma density and temperature. The exact analytical solution obtained in this work is seen to be useful for addressing this question in future work too.

Supplementary Information The online version contains supplementary material available at https://doi.org/10.1007/s11207-021-01841-1.

Acknowledgments The work was supported in part by the Ministry of Science and Higher Education of the Russian Federation by State assignment to educational and research institutions under Projects No. FSSS-2020-0014, 0023-2019-0003, and by Subsidy No.075-GZ/C3569/278. D.Y. Kolotkov acknowledges support from the STFC consolidated grant ST/T000252/1.

Declarations

Disclosure of Potential Conflicts of Interest The authors declare that they have no conflicts of interest.

References

Afanasyev, A.N., Nakariakov, V.M.: 2015, Nonlinear slow magnetoacoustic waves in coronal plasma structures. *Astron. Astrophys.* **573**, A32. DOI. ADS.

Andries, J., Arregui, I., Goossens, M.: 2005, Determination of the coronal density stratification from the observation of harmonic coronal loop oscillations. *Astrophys. J. Lett.* **624**, L57. DOI. ADS.

Antolin, P.: 2020, Thermal instability and non-equilibrium in solar coronal loops: from coronal rain to long-period intensity pulsations. *Plasma Phys. Control. Fusion* **62**, 014016. DOI. ADS.
Antolin, P., Shibata, K., Vissers, G.: 2010, Coronal rain as a marker for coronal heating mechanisms. *Astrophys. J.* **716**, 154. DOI. ADS.
Banerjee, D., Gupta, G.R., Teriaca, L.: 2011, Propagating MHD waves in coronal holes. *Space Sci. Rev.* **158**, 267. DOI. ADS.
Banerjee, D., Krishna Prasad, S.: 2016, MHD waves in coronal holes. In: Keiling, A., Lee, D.-H., Nakariakov, V. (eds.) *Low-Frequency Waves in Space Plasmas, Geophys. Mono. Ser.* **216**, 419. DOI. ADS.
Botha, G.J.J., Arber, T.D., Nakariakov, V.M., Zhugzhda, Y.D.: 2011, Chromospheric resonances above sunspot umbrae. *Astrophys. J.* **728**, 84. DOI. ADS.
Chin, R., Verwichte, E., Rowlands, G., Nakariakov, V.M.: 2010, Self-organization of magnetoacoustic waves in a thermally unstable environment. *Phys. Plasmas* **17**, 032107. DOI. ADS.
Claes, N., Keppens, R.: 2019, Thermal stability of magnetohydrodynamic modes in homogeneous plasmas. *Astron. Astrophys.* **624**, A96. DOI. ADS.
De Moortel, I.: 2009, Longitudinal waves in coronal loops. *Space Sci. Rev.* **149**, 65. DOI. ADS.
De Moortel, I., Hood, A.W.: 2003, The damping of slow MHD waves in solar coronal magnetic fields. *Astron. Astrophys.* **408**, 755. DOI. ADS.
De Moortel, I., Hood, A.W.: 2004, The damping of slow MHD waves in solar coronal magnetic fields. II. The effect of gravitational stratification and field line divergence. *Astron. Astrophys.* **415**, 705. DOI. ADS.
Duckenfield, T.J., Kolotkov, D.Y., Nakariakov, V.M.: 2021, The effect of the magnetic field on the damping of slow waves in the solar corona. *Astron. Astrophys.* **646**, A155. DOI. ADS.
Fang, X., Xia, C., Keppens, R.: 2013, Multidimensional modeling of coronal rain dynamics. *Astrophys. J. Lett.* **771**, L29. DOI. ADS.
Field, G.B.: 1965, Thermal instability. *Astrophys. J.* **142**, 531. DOI. ADS.
Goossens, M.L., Arregui, I., Van Doorsselaere, T.: 2019, Mixed properties of MHD waves in non-uniform plasmas. *Front. Astron. Space Sci.* **6**, 20. DOI. ADS.
Heyvaerts, J.: 1974, The thermal instability in a magnetohydrodynamic medium. *Astron. Astrophys.* **37**, 65. ADS.
Kaneko, T., Yokoyama, T.: 2017, Reconnection-condensation model for solar prominence formation. *Astrophys. J.* **845**, 12. DOI. ADS.
Kohutova, P., Verwichte, E.: 2017, Dynamics of plasma condensations in a gravitationally stratified coronal loop. *Astron. Astrophys.* **602**, A23. DOI. ADS.
Kohutova, P., Antolin, P., Popovas, A., Szydlarski, M., Hansteen, V.H.: 2020, Self-consistent 3D radiative magnetohydrodynamic simulations of coronal rain formation and evolution. *Astron. Astrophys.* **639**, A20. DOI. ADS.
Kolotkov, D.Y., Duckenfield, T.J., Nakariakov, V.M.: 2020, Seismological constraints on the solar coronal heating function. *Astron. Astrophys.* **644**, A33. DOI. ADS.
Kolotkov, D.Y., Nakariakov, V.M., Zavershinskii, D.I.: 2019, Damping of slow magnetoacoustic oscillations by the misbalance between heating and cooling processes in the solar corona. *Astron. Astrophys.* **628**, A133. DOI. ADS.
Krishna Prasad, S., Banerjee, D., Van Doorsselaere, T.: 2014, Frequency-dependent damping in propagating slow magneto-acoustic waves. *Astrophys. J.* **789**, 118. DOI. ADS.
Krishna Prasad, S., Jess, D.B., Van Doorsselaere, T.: 2019, The temperature-dependent damping of propagating slow magnetoacoustic waves. *Front. Astron. Space Sci.* **6**, 57. DOI. ADS.
Krishna Prasad, S., Raes, J.O., Van Doorsselaere, T., Magyar, N., Jess, D.B.: 2018, The polytropic index of solar coronal plasma in sunspot fan loops and its temperature dependence. *Astrophys. J.* **868**, 149. DOI. ADS.
Kupriyanova, E., Kolotkov, D., Nakariakov, V., Kaufman, A.: 2020, Quasi-periodic pulsations in solar and stellar flares. Review. *J. Solar-Terr. Phys.* **6**, 3. DOI. ADS.
Luna-Cardozo, M., Verth, G., Erdélyi, R.: 2012, Longitudinal oscillations in density stratified and expanding solar waveguides. *Astrophys. J.* **748**, 110. DOI. ADS.
Mandal, S., Magyar, N., Yuan, D., Van Doorsselaere, T., Banerjee, D.: 2016, Forward modeling of propagating slow waves in coronal loops and their frequency-dependent damping. *Astrophys. J.* **820**, 13. DOI. ADS.
McEwan, M.P., Donnelly, G.R., Díaz, A.J., Roberts, B.: 2006, On the period ratio $P_1/2P_2$ in the oscillations of coronal loops. *Astron. Astrophys.* **460**, 893. DOI. ADS.
McLaughlin, J.A., Nakariakov, V.M., Dominique, M., Jelínek, P., Takasao, S.: 2018, Modelling quasi-periodic pulsations in solar and stellar flares. *Space Sci. Rev.* **214**, 45. DOI. ADS.
Molevich, N.E., Oraevskii, A.N.: 1988, Second viscosity in thermodynamically nonequilibrium media. *Zh. Eksp. Teor. Fiz.* **94**, 128. [*J. Exp. Theor. Phys.* **67**, 504 (1988)].

Molevich, N.E., Ryashchikov, D.S.: 2020, Autowave pulse in a medium with the heating/cooling misbalance and an arbitrary thermal dispersion. *Tech. Phys. Lett.* **46**, 637. DOI. ADS.
Molevich, N.E., Zavershinskiy, D.I., Ryashchikov, D.S.: 2016, Investigation of the mhd wave dynamics in thermally unstable plasma. *Magnetohydrodynamics* **52**, 191. DOI.
Molevich, N.E., Zavershinsky, D.I., Galimov, R.N., Makaryan, V.G.: 2011, Traveling self-sustained structures in interstellar clouds with the isentropic instability. *Astrophys. Space Sci.* **334**, 35. DOI. ADS.
Murawski, K., Zaqarashvili, T.V., Nakariakov, V.M.: 2011, Entropy mode at a magnetic null point as a possible tool for indirect observation of nanoflares in the solar corona. *Astron. Astrophys.* **533**, A18. DOI. ADS.
Nakariakov, V.M., Kolotkov, D.Y.: 2020, Magnetohydrodynamic waves in the solar corona. *Annu. Rev. Astron. Astrophys.* **58**, 441. DOI. ADS.
Nakariakov, V.M., Mendoza-Briceño, C.A., Ibáñez S., M.H.: 2000, Magnetoacoustic waves of small amplitude in optically thin quasi-isentropic plasmas. *Astrophys. J.* **528**, 767. DOI. ADS.
Nakariakov, V.M., Afanasyev, A.N., Kumar, S., Moon, Y.-J.: 2017, Effect of local thermal equilibrium misbalance on long-wavelength slow magnetoacoustic waves. *Astrophys. J.* **849**, 62. DOI. ADS.
Nakariakov, V.M., Kosak, M.K., Kolotkov, D.Y., Anfinogentov, S.A., Kumar, P., Moon, Y.-J.: 2019, Properties of slow magnetoacoustic oscillations of solar coronal loops by multi-instrumental observations. *Astrophys. J. Lett.* **874**, L1. DOI. ADS.
Nisticò, G., Polito, V., Nakariakov, V.M., Del Zanna, G.: 2017, Multi-instrument observations of a failed flare eruption associated with MHD waves in a loop bundle. *Astron. Astrophys.* **600**, A37. DOI. ADS.
Ofman, L., Wang, T.: 2002, Hot coronal loop oscillations observed by SUMER: slow magnetosonic wave damping by thermal conduction. *Astrophys. J. Lett.* **580**, L85. DOI. ADS.
Ofman, L., Wang, T.J., Davila, J.M.: 2012, Slow magnetosonic waves and fast flows in active region loops. *Astrophys. J.* **754**, 111. DOI. ADS.
Owen, N.R., De Moortel, I., Hood, A.W.: 2009, Forward modelling to determine the observational signatures of propagating slow waves for TRACE, SoHO/CDS, and Hinode/EIS. *Astron. Astrophys.* **494**, 339. DOI. ADS.
Polyanin, A.D., Zaitsev, V.F.: 2002, *Handbook of Exact Solutions for Ordinary Differential Equations*, Chapman and Hall/CRC press. ADS.
Prasad, A., Srivastava, A.K., Wang, T.J.: 2021, Role of compressive viscosity and thermal conductivity on the damping of slow waves in coronal loops with and without heating-cooling imbalance. *Solar Phys.* **296**, 20. DOI. ADS.
Provornikova, E., Ofman, L., Wang, T.: 2018, Excitation of flare-induced waves in coronal loops and the effects of radiative cooling. *Adv. Space Res.* **61**, 645. DOI. ADS.
Reale, F.: 2016, Plasma sloshing in pulse-heated solar and stellar coronal loops. *Astrophys. J. Lett.* **826**, L20. DOI. ADS.
Reale, F., Lopez-Santiago, J., Flaccomio, E., Petralia, A., Sciortino, S.: 2018, X-ray flare oscillations track plasma sloshing along star-disk magnetic tubes in the Orion star-forming region. *Astrophys. J.* **856**, 51. DOI. ADS.
Reale, F., Testa, P., Petralia, A., Kolotkov, D.Y.: 2019, Large-amplitude quasiperiodic pulsations as evidence of impulsive heating in hot transient loop systems detected in the EUV with SDO/AIA. *Astrophys. J.* **884**, 131. DOI. ADS.
Riedl, J.M., Van Doorsselaere, T., Santamaria, I.C.: 2019, Wave modes excited by photospheric p-modes and mode conversion in a multi-loop system. *Astron. Astrophys.* **625**, A144. DOI. ADS.
Ruderman, M.S.: 2006, Nonlinear waves in the solar atmosphere. *Phil. Trans. Roy. Soc. London Ser. A* **364**, 485. DOI. ADS.
Ryashchikov, D.S., Molevich, N.E., Zavershinskii, D.I.: 2017, Characteristic times of acoustic and condensation instability in heat-releasing gas media. *Proc. Eng.* **176**, 416. DOI.
Selwa, M., Murawski, K., Solanki, S.K.: 2005, Excitation and damping of slow magnetosonic standing waves in a solar coronal loop. *Astron. Astrophys.* **436**, 701. DOI. ADS.
Somov, B.V., Dzhalilov, N.S., Staude, J.: 2007, Peculiarities of entropy and magnetosonic waves in optically thin cosmic plasma. *Astron. Lett.* **33**, 309. DOI. ADS.
Van Doorsselaere, T., Kupriyanova, E.G., Yuan, D.: 2016, Quasi-periodic pulsations in solar and stellar flares: an overview of recent results (invited review). *Solar Phys.* **291**, 3143. DOI. ADS.
Van Doorsselaere, T., Wardle, N., Del Zanna, G., Jansari, K., Verwichte, E., Nakariakov, V.M.: 2011, The first measurement of the adiabatic index in the solar corona using time-dependent spectroscopy of Hinode/EIS observations. *Astrophys. J. Lett.* **727**, L32. DOI. ADS.
Verwichte, E., Haynes, M., Arber, T.D., Brady, C.S.: 2008, Damping of slow MHD coronal loop oscillations by shocks. *Astrophys. J.* **685**, 1286. DOI. ADS.
Wang, T.: 2011, Standing slow-mode waves in hot coronal loops: observations, modeling, and coronal seismology. *Space Sci. Rev.* **158**, 397. DOI. ADS.

Wang, T.J.: 2016, Waves in solar coronal loops. In: Keiling, A., Lee, D.-H., Nakariakov, V. (eds.) *Low-Frequency Waves in Space Plasmas, Geophys. Mono. Ser.* **216**, Am. Geophys. Union, Washington, 395. DOI. ADS.

Wang, T., Ofman, L.: 2019, Determination of transport coefficients by coronal seismology of flare-induced slow-mode waves: numerical parametric study of a 1D loop model. *Astrophys. J.* **886**, 2. DOI. ADS.

Wang, T., Ofman, L., Davila, J.M.: 2013, Three-dimensional magnetohydrodynamic modeling of propagating disturbances in fan-like coronal loops. *Astrophys. J. Lett.* **775**, L23. DOI. ADS.

Wang, T., Ofman, L., Sun, X., Provornikova, E., Davila, J.M.: 2015, Evidence of thermal conduction suppression in a solar flaring loop by coronal seismology of slow-mode waves. *Astrophys. J. Lett.* **811**, L13. DOI. ADS.

Wang, T., Ofman, L., Sun, X., Solanki, S.K., Davila, J.M.: 2018, Effect of transport coefficients on excitation of flare-induced standing slow-mode waves in coronal loops. *Astrophys. J.* **860**, 107. DOI. ADS.

Wang, T., Ofman, L., Yuan, D., Reale, F., Kolotkov, D.Y., Srivastava, A.K.: 2021, Slow-mode magnetoacoustic waves in coronal loops. *Space Sci. Rev.* **217**, 34. DOI. ADS.

Yuan, D., Nakariakov, V.M.: 2012, Measuring the apparent phase speed of propagating EUV disturbances. *Astron. Astrophys.* **543**, A9. DOI. ADS.

Zavershinskii, D.I., Kolotkov, D.Y., Nakariakov, V.M., Molevich, N.E., Ryashchikov, D.S.: 2019, Formation of quasi-periodic slow magnetoacoustic wave trains by the heating/cooling misbalance. *Phys. Plasmas* **26**, 082113. DOI. ADS.

Zavershinskii, D.I., Molevich, N.E., Riashchikov, D.S., Belov, S.A.: 2020, Nonlinear magnetoacoustic waves in plasma with isentropic thermal instability. *Phys. Rev. E* **101**, 043204. DOI. ADS.

Zavershinsky, D.I., Molevich, N.E.: 2013, A magnetoacoustic autowave pulse in a heat-releasing ionized gaseous medium. *Tech. Phys. Lett.* **39**, 676. DOI. ADS.

Publisher's Note Springer Nature remains neutral with regard to jurisdictional claims in published maps and institutional affiliations.

Authors and Affiliations

D. Zavershinskii[1,2] · D. Kolotkov[3,4] · D. Riashchikov[1,2] · N. Molevich[2]

✉ D. Zavershinskii
dimanzav@mail.ru

1 Department of Physics, Samara National Research University, Moscovskoe sh. 34, Samara, 443086, Russia

2 Department of Theoretical Physics, Lebedev Physical Institute, Novo-Sadovaya st. 221, Samara, 443011, Russia

3 Centre for Fusion, Space and Astrophysics, Department of Physics, University of Warwick, Coventry, CV4 7AL, UK

4 Institute of Solar-Terrestrial Physics SB RAS, Irkutsk, 664033, Russia